Scaling properties of cracks

1997 J. Phys.: Condens. Matter 9 4319

(http://iopscience.iop.org/0953-8984/9/21/002)

J. Phys.: Condens. Matter **9** (1997) 4319–4344. Printed in the UK PII: S0953-8984(97)72446-9

REVIEW ARTICLE

Scaling properties of cracks

Elisabeth Bouchaud

ONERA (OM), 29 Avenue de la Division Leclerc, BP 72, F-92322 Châtillon Cédex, France

Received 29 November 1996

Abstract. Experiments concerning the morphology of fracture surfaces of various materials are reviewed. The observations are interpreted within the framework of models of lines moving in a random environment. This suggests that fracture of heterogeneous materials could be seen as a dynamic phase transition.

Fractography has always been a useful tool for the understanding of fracture mechanisms in complex materials. Microstructural heterogeneities—grain boundaries, second phase precipitates, dislocation assemblies, ...—control the ability of the material to resist crack initiation or propagation, and can be identified on the fracture surface as more or less easy paths for cracks. Hence, when a quantitative analysis of fracture surfaces was made possible by technical progress in image analysis, naturally an attempt was made to correlate the measured roughness with macroscopic mechanical properties. It was in 1984 that, for the first time, Mandelbrot *et al* [1] characterized the 'fractal' self-affinity [2–4] of fracture surfaces of a steel. After their pioneering work, other materials—mainly steels [5, 6] and ceramics [7–9]—were examined, by the same experimental method. Correlations were claimed to be established between the value of the roughness exponent ζ [2, 3] (lying usually between 0.7 and 0.9), and the fracture toughness K_{Ic} of the material, which measures its resistance against crack propagation. This is still a somewhat controversial topic, although it was conjectured in 1990 [10], on the basis of experiments performed using a slightly different experimental procedure [11] on an aluminium alloy, that $\zeta \simeq 0.8$ is a *universal* exponent. This conjecture has been confirmed by many experiments since then [12–19], for all sorts of materials, both brittle and ductile, analysed using various experimental techniques. There seems to be in each case a scaling domain—which is very much material [20] dependent—in which this roughness exponent is observed.

At smaller length scales of observation, however—typically on the nanometre scale, for metallic alloys, whereas the universal exponent (the above value $\zeta \sim 0.8$) is usually observed in the micrometre–millimetre range—significantly smaller exponents have been reported, first by Milman *et al* [21, 22] using a scanning tunnelling microscope (STM) for a few materials. On the other hand, McAnulty *et al* [23] performed two types of fracture experiments on the same steel. Charpy tests [24]—one just throws a hammer into a notch in the material: in this case, crack propagation should be rather brutal and quick—gave rise to a roughness index quite close to 0.8. In contrast, low-cycle fatigue tests, which may be thought of as a slower process, led to a smaller roughness index ($\simeq$0.6).

The very existence of two regimes, the extension of which seems to depend on the propagation speed, is reminiscent of the pinning/depinning transition [25–28] of lines moving through randomly distributed impurities [29–32], which have been extensively studied

0953-8984/97/214319+26$19.50

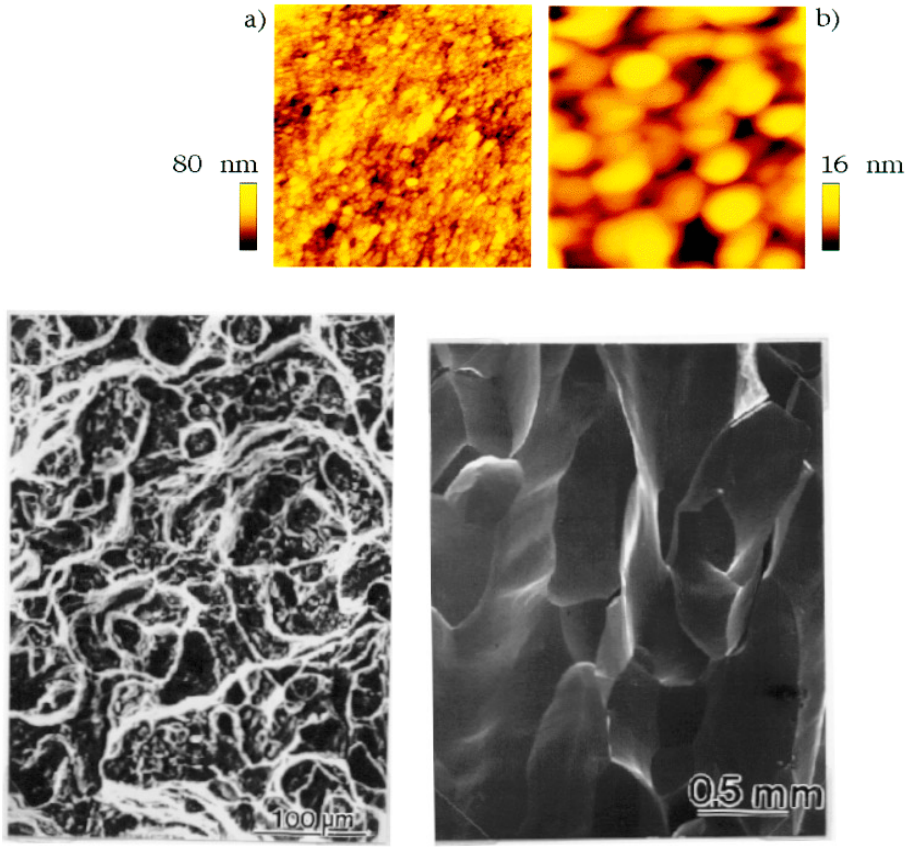

Figure 1. Fracture surfaces of various materials. (a), (b) AFM images of the end of the mirror zone in soda-lime float glass (courtesy of F Creuzet [18, 19]). (a) 5 μm $\times$ 5 μm. (b) 375 nm $\times$ 375 nm. Rather well defined entities can be seen on the fracture surface, the height of which can be reliably measured as in the range of a few nanometres. However, their apparent width (tens of nanometres) may be the consequence of artifacts if the radius of curvature of the tip is considered (typically 20 nm). (c) A fracture surface of 7475 aluminium alloy (a SEM micrograph). (d) A fracture surface of polycrystalline Ni_3Al (a SEM micrograph). (e) A fracture surface of granite (courtesy of J-P Hulin; photograph by C Grisot). Brittle fracture (glass, granite, intergranular fracture of Ni_3Al) leads to 'shallower' surfaces than ductile fracture (aluminium alloy).

during these last few years. In fact, it has been suggested, in [33], that these models might be relevant for describing the propagation of crack fronts in heterogeneous materials: understanding the morphology of the crack front at a given time allows one to infer the features of the fracture surface, which is simply its trace left behind. Although these models still suffer from some weaknesses as regards the description of crack fronts, most of them lead to some interesting predictions, which can be summarized as follows. For crack velocities tending to zero, i.e. when the force pulling the line is close to the critical force for which the crack front is just able to free itself from the microstructural obstacles, the roughness index of the

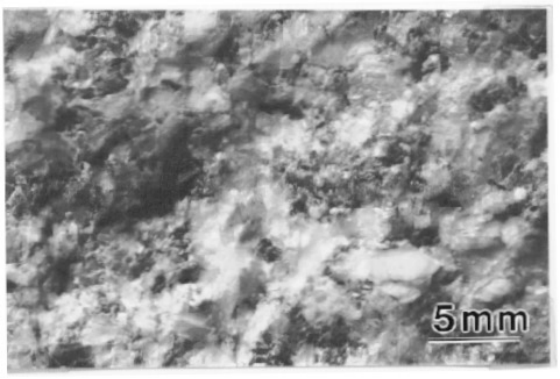

(e)

Figure 1. (Continued)

fracture surface is characteristic of the vicinity of this so-called 'depinning transition'. For non-zero crack velocities, this behaviour is recovered at small length scales, while at larger ones, a new regime appears, characterized by a different roughness exponent. The crossover length separating the two regimes decreases as a power law with increasing crack velocity.

Some experiments which are briefly described in the following have shown that, in fact, the roughness index of the small-length-scales regime is indeed close to 0.5, whereas at larger length scales, the *universal* value 0.8 is recovered [34–36]. This scenario is also supported by recent molecular dynamics (MD) simulations on the fracture of amorphous materials due to Kalia and Vashishta's team [37–40]. These scaling properties could even be observed over five decades of length scales thanks to the simultaneous use of a standard scanning electron microscope (SEM) and of an atomic force microscope (AFM) [35, 36]. However, making quantitative measurements of the average crack velocity both for the fatigue of metals and for the stress corrosion of glass has only recently become possible. These new results strongly support the description of crack advance in terms of line propagation in a random environment.

This unachieved play, where some characters hope to introduce crack propagation into the large group of dynamic critical phenomena, unfolds here. Act I describes the epopee of the pioneers, after a very brief review of self-affine surfaces and the methods for analysing them. Act II illustrates the struggle of the universalists, and the jeopardizing of their position by STM experiments. Act III summarizes the predictions of the line pinning/depinning models, as well as the results of MD simulations. Finally, Act IV describes the most recent observations, spanning over five decades of length-scale studies in some cases, which led to an analysis of the morphology of fracture surfaces as a function of crack velocity. Yet, there is no epilogue to the play—only partial conclusions which ask for more work to lead to a deeper understanding of the true nature of crack propagation in heterogeneous media.

Act I—the pioneers

Fracture surfaces may have different aspects, but usually look like mountain landscapes, with peaks and valleys at various scales of observation (see figure 1). To the eye however, the fracture surfaces of brittle materials such as granite or glass seem less 'rough' than the fracture surface of a ductile metallic alloy (figure 1). Thus, in order to correlate the

measured roughness with the material's properties, it is very tempting to analyse their self-affinity [2, 3]. This is what Mandelbrot and collaborators [1] did for the first time. Before their experimental results are reported, the definition of self-affinity is briefly recalled, and the main methods for measuring roughness indices are indicated.

Scene 1. The scene takes place in some strange mountains: self-affine surfaces

The notion of self-affinity was used first to characterize the Brownian fractional reliefs, introduced by Mandelbrot and Van Ness [41, 2]. Unlike self-similar objects, self-affine structures, being intrinsically anisotropic, are not statistically invariant through a global dilation but rather through an affine transformation:

$$(x, y, z) \longrightarrow (bx, by, b^{\zeta} z) \tag{1}$$

where z is the height, and x and y are the coordinates within the plane perpendicular to the z-direction, which will be called 'horizontal' in the following. ζ is the so-called *roughness index* or *Hurst exponent*. Equation (1) implies in general that the typical height $h(r)$ at point $r = \sqrt{x^2 + y^2}$ is given by

$$h(r) = \langle (z(r_0 + r) - z(r_0))^2 \rangle_{r_0}^{1/2} \simeq r^{\zeta}. \tag{2}$$

ζ lies between the values 0 and 1, and is related to the fractal dimension (the 'box dimension' [2]) of the whole structure through the relation

$$d_F = 3 - \zeta. \tag{3}$$

$\zeta = 1$ corresponds to a regular surface, inclined with respect to the horizontal plane: one climbs a height $h(r)$ just proportional to the distance r travelled in the horizontal plane (equation (2)). Hence, it corresponds to a fractal dimension $d_F = 2$. Paradoxically enough, the smaller ζ, the rougher the surface (the larger the fractal dimension d_F); these scaling properties are to be understood at *small* length scales r. A self-affine surface is indeed fractal up to distances of the order of a characteristic length called the *correlation length* ξ, beyond which the object is flat, and its dimension is simply equal to 2.

One property of these structures which is of practical importance is the so-called *return probability* [42] $P_0(r)$, which is the probability that z returns to its initial value $z(r = 0) = 0$ after a distance r is travelled in the 'horizontal' plane. It can be shown that

$$P_0(r) \propto r^{-\zeta}. \tag{4}$$

Experimentally, except in a few cases, one usually has to produce a cut of the fracture surface. This cut may either be perpendicular to the z-axis (one then gets contour lines), or contain it. In the latter case, one may directly compute P_0 or the *first* return probability P_1 (the probability that the height returns *first* to its initial value after a distance r is travelled) [42, 43], or any moment of the z-distribution on the fracture profile. One particularly reliable quantity is

$$z_{max}(r) = \langle \mathrm{Max}\{z(r')\}_{x<r'<x+r} - \mathrm{Min}\{z(r')\}_{x<r'<x+r} \rangle_x \propto r^{\zeta}. \tag{5}$$

On the other hand, the intersection of the self-affine surface with a plane $z = 0$ is a self-similar object of dimension $d_F - 1$. Thus,

$$\mathcal{C}(r) \propto \frac{1}{r^{d-(d_F-1)}} = \frac{1}{r^{2-(2-\zeta)}} = r^{-\zeta}. \tag{6}$$

In fact, $P_0(r)$ is the probability of finding a point of the surface within that plane, i.e. belonging to the intersection, knowing that there was one at $r = 0$. In other words, $P_0(r)$ is indeed the self-correlation function $\mathcal{C}(r)$ of the intersection. This property lies at the

origin of all of the experimental procedures which use cuts of the surface by a $z =$ constant plane, and it is the basis, in particular, of the *slit island method* introduced by Mandelbrot and collaborators [1].

Scene 2. The epopee of the pioneers in the self-affine mountains

Mandelbrot, Passoja and Paullay [1] studied six samples of steel to which different heat treatments had conferred different fracture energies, measured through Charpy tests [24]. To analyse the resulting fracture surfaces, these were plated with vacuum-deposited nickel, and subsequently cut and polished within a $z =$ constant plane. Images of the 'islands' of steel emerging from an 'ocean' of nickel were analysed, and both the area $\mathcal{A}$ and the perimeter $\mathcal{P}$ of the islands were measured. The islands themselves are dense bidimensional objects, but as their contours are the intersections of the fracture surface with a $z =$ constant plane, they have a dimension $d_F - 1$ if the surface itself is self-affine of dimension d_F. Thus, $\mathcal{A} \propto l^2$ and $\mathcal{P} \propto l^{(d_F-1)}$, where l is the linear size of the islands considered; hence,

$$\mathcal{A} \propto \mathcal{P}^{2/(d_F-1)}. \tag{7}$$

Plotting $\mathcal{A}$ versus $\mathcal{P}$ on a log–log plot should then show two linearly increasing regimes. At length scales smaller than the correlation length ξ, one should measure a slope $2/(2-\zeta)$, and one should measure a slope 2 at larger length scales. Note that with this method of measurement, a slight overestimation of ξ leads to an overestimation of the slope, and hence to an underestimation of ζ.

The measured values of ζ lay between 0.70 and 0.85. The authors' conclusion was that ζ was increasing with decreasing fracture energy; unexpectedly, this meant that rougher fracture surfaces corresponded to lower fracture energies.

This experimental method has been extensively used since that first experiment, especially on steels, and on ceramics. The roughness indices, evaluated in scaling regimes spanning over barely two decades, lie between 0.7 and 0.9. Unfortunately, it can be shown that the precision of the measured roughness exponents is rather poor, especially when the scaling domain is small. It is even worse if there exist two regimes, characterized by two different exponents [36], as will be shown in the following. Nevertheless, a correlation was claimed to exist in each case with the fracture toughness, which relates rougher surfaces to higher fracture energies—or the other way round! These correlations were first questioned on the basis of the results of experiments performed on a commercial aluminium alloy. With reference [10] began the War of Secession between the correlationists and the universalists.

Act II—the battle of the universalists

Measurements comparable to those done by Mandelbrot *et al* [1] were performed on a commercial aluminium alloy called 7475—using a different experimental procedure, however. Four samples were studied, to which different solution heat treatments and quenches conferred different fracture toughnesses. K_{Ic} was measured on CT (compact tension) specimens (see figure 2(a)) first precracked in fatigue. The tensile fracture surfaces (see figure 1(c)) were electrochemically nickel plated—a route which is far less directional than vacuum evaporation—and polished surfaces corresponding to cuts by $z =$ constant planes were observed at various magnifications with a SEM, using backscattered electrons which give a very good contrast between aluminium and nickel. A sketch of the experimental procedure is shown in figure 2(b).

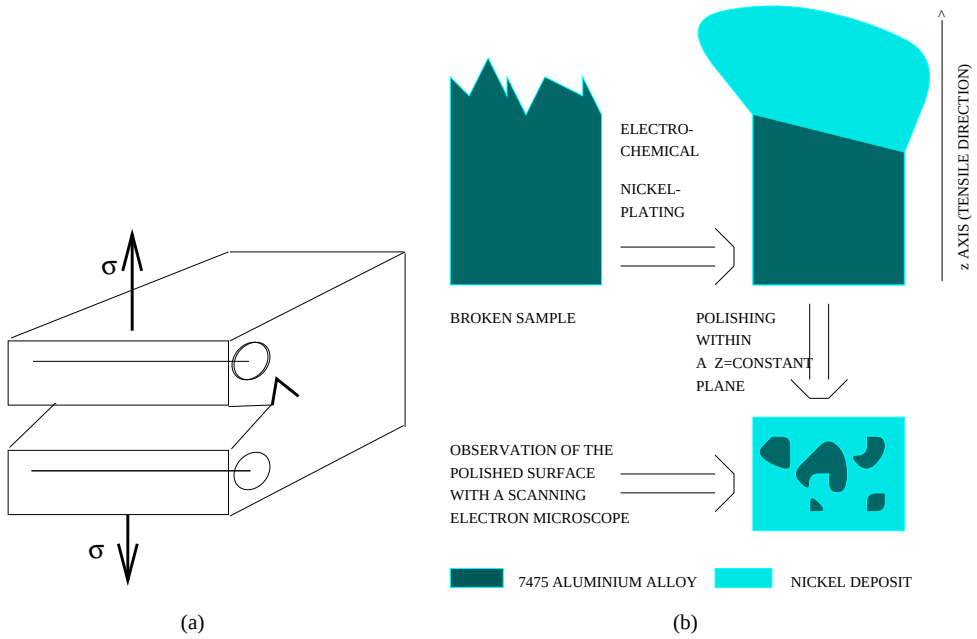

Figure 2. (a) A compact tension (CT) sample, subjected to mode I crack propagation (the plane of the crack is perpendicular to the tensile axis). (b) A sketch of the experimental procedure: the fracture surfaces are electrochemically plated with Ni, and polished within a $z =$ constant plane. When profiles are required, the plated samples are polished within a plane containing the z-axis. Observations are performed with a SEM (backscattered-electron contrast) at various magnifications.

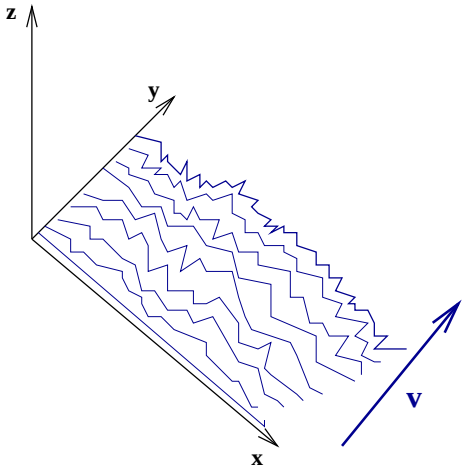

Figure 3. A line moving along the y-axis, leaving behind it a rough surface. xy is the plane of propagation.

The self-correlation functions $\mathcal{C}(r)$ of the cuts were computed for each micrograph from the binarized image. $\mathcal{C}(r)$ was shown to exhibit a power-law decrease extending up to a size Λ comparable to the size of the micrograph itself. The curves relating to the

same sample were put on the same diagram by plotting $\mathcal{C}(r)$ versus r/Λ. In these reduced units, the scaling domain extended over two decades, corresponding to three decades on the actual scale: $0.5\ \mu\text{m} < r < 0.5$ mm. The exponents were measured in each case, and no systematic variation of ζ with K_{Ic} was observed:

$$\zeta = 0.80 \pm 0.05. \tag{8}$$

It could not be concluded that there was any correlation between the roughness exponent and the fracture toughness, and it was proposed that this exponent might be *universal*, i.e. independent of the fracture mode, fracture toughness, and material. It was argued that the differences in the measured 'apparent' exponents could be due to differences in the correlation lengths, which are believed to depend strongly on the microstructure (see figure 1). The first battle of the War of Secession had begun.

The first reinforcements for the universalists arrived in 1992, with the experiments of Måly and co-workers [12]. These authors studied six very different brittle materials (plaster, Bakelite, porcelain, graphite, steel, and Al–Si) by recording the fracture profiles using an optomechanical profilometer. By computing both the first return probability $P_1(r)$ (see Act I, scene 1) and the power spectrum, they found consistent values of ζ which did not vary much from one material to the other, and they concluded that ζ seemed indeed to be *universal*:

$$\zeta = 0.87 \pm 0.07. \tag{9}$$

This result is compatible with equation (8), and the differences may be explained by the strong sensitivity of both the self-affine correlation length ξ, and the length ξ_c of crossover to the small-length-scales regime (see below, Acts III and IV).

Other systems were investigated after these, giving results very similar to (8) and (9): a viscoelastic paste made of sand and resin was studied by Lemaire and co-workers [13], mode II branched cracks in polycrystalline Ni_3Al [14] and rocks [15, 16] were investigated also, and results on steel obtained by the electrochemical method were reported by Imre *et al* [17].

For some time, it seemed that the universalists would win the war. But the opposing army found a very efficient weapon called STM. With this, they were able to analyse fracture surfaces of metallic materials at the nanometre scale. The values that they reported were significantly smaller than the universal exponent, lying generally between 0.4 and 0.6. It could well be argued that non-universal behaviours could arise at such small length scales, but this result, together with the observations of McAnulty and co-workers [23], actually fits with the predictions of the line-moving models in the vicinity of the so-called depinning transition.

Act III—models of lines moving in random environments: *deus ex machina*?

It is quite natural to imagine a fracture front as a line moving through a material containing randomly distributed microstructural obstacles, separating the specimen into two broken pieces as it moves along its path. The morphology of the line at each time t determines the morphology of the final fracture surfaces, which are the surfaces of these broken pieces. It was only suggested first in [33] that the work of Ertaş and Kardar [30] might be applicable to fracture. The pinning/depinning transition has been the subject of many theoretical studies in recent years, both for propagating lines and for growing interfaces in a random environment. Various models, both two and three dimensional, have been developed for calculating the critical exponents characterizing fronts in a plane or surfaces in real space.

For a line moving within a plane, a general equation can be written, in which the velocity normal to the interface, proportional to $\langle \partial z/\partial t \rangle$ (see figure 3), is equated to the sum of a curvature force, a random quenched force $\eta(x, z)$ accounting for the presence of uncorrelated random pinning obstacles, and a pulling force F. Several cases may arise. The pulling force F has to reach a threshold F_c for the line to be able to move. Below this threshold, the line is pinned by microstructural obstacles, and its morphology strongly depends on its history. When F is equal to F_c, the line is just able to free itself from the pinning obstacles, but its velocity is still equal to zero. It is self-affine, and its roughness index ζ_c is believed to be independent of the precise nature of the pinning forces. Similarly, the dynamic exponent z_c describing the short-time evolution of the height fluctuations:

$$\langle (z(x,t) - z(x',t'))^2 \rangle \propto |x - x'|^{2\zeta_c} f\left(\frac{t - t'}{|x - x'|^{z_c}} \right) \tag{10}$$

is also universal. One has: $f(y \to 0) =$ constant and $f(y \gg 1) = y^{2\zeta_c/z_c}$.

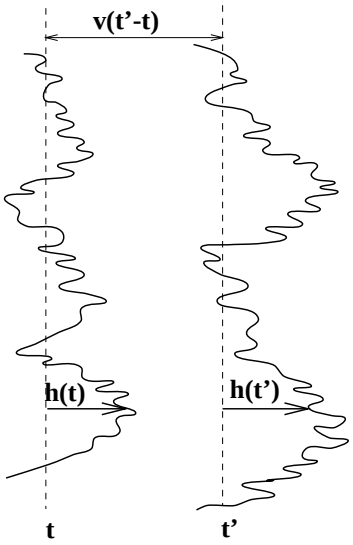

Figure 4. The moving line at times t and t'. One can indeed see the line moving if the fluctuations of height are not too strong, i.e. if $v(t' - t) > |h(x, t') - h(x, t)|$ (equation (12)). This is true for length scales larger than $\xi_c \sim v^{-1/(z_c - \zeta_c)}$ (equation (18)), or at times longer than $\Delta t \sim (1/v)^{z_c/(z_c - \zeta_c)}$ (equation (14)).

Beyond the threshold, i.e. when the mean line velocity v is non-zero, one can write: $z = vt + h(x, t)$. In the moving frame, the random forces act as a thermal noise: $\eta(x, z) \simeq \eta(x, vt)$. In this case, for a line moving in two dimensions, Kardar, Parisi and Zhang [44] showed that, for non-pathological noise distributions (peaked distributions), the roughness and dynamic exponents are respectively

$$\zeta = \frac{1}{2} \qquad z = \frac{3}{2}. \tag{11}$$

We will now use an argument due to Leshhorn *et al* [45] to give a feeling for what happens at small length scales (or equivalently, at short times) for a non-zero value of v. For the movement of the line to be observable during a long time interval $t' - t$ (see figure 4), the

fluctuations of z have to be negligible when compared to $v(t'-t)$:

$$v(t'-t) > |h(x,t') - h(x,t)|. \tag{12}$$

Because (see equation (10)) $|h(x,t') - h(x,t)| \simeq (t'-t)^{\zeta_c/z_c}$, equation (12) requires that

$$\frac{\zeta_c}{z_c} < 1. \tag{13}$$

From equation (12), a time-scale $\Delta t = t' - t$ can be defined for which the height fluctuations are of the same order of magnitude as the mean variation of z. In this case (equations (10) and (12)) $\Delta t^{1-\zeta_c/z_c} \simeq 1/v$; hence

$$\Delta t \sim \left(\frac{1}{v}\right)^{z_c/(z_c-\zeta_c)}. \tag{14}$$

To this time-scale corresponds a length scale:

$$\xi_c \sim \Delta t^{1/z_c} \sim v^{-1/(z_c-\zeta_c)} \tag{15}$$

below which the average movement of the line at a velocity v is not observable. At small length scales, although $v > 0$, the line can thus be considered to be at threshold.

Since v depends on the distance to the overall threshold force F_c:

$$v \sim (F - F_c)^{\beta} \tag{16}$$

equation (15) can be written as

$$\xi_c \sim (F - F_c)^{-\nu} \tag{17}$$

with

$$\nu = -\frac{\beta}{z_c - \zeta_c}. \tag{18}$$

As expected, ξ_c diverges when F is equal to F_c: the whole line is then at threshold.

Ertaş and Kardar studied a local non-linear three-dimensional Langevin equation for describing the morphology of polymers in shear flows [30] or the motion of flux lines [31]. These equations deal separately with the fluctuations of the line parallel to the line velocity and to the pulling force ($\|$) and with those perpendicular to it ($\perp$) (see figure 5):

$$\frac{\partial h_\|}{\partial t} = \lambda_\| \left(\frac{\partial h_\|}{\partial x}\right)^2 + \lambda_x \left(\frac{\partial h_\|}{\partial x}\frac{\partial h_\perp}{\partial x}\right) + \Delta h_\| + \eta_\|(x,t) \tag{19a}$$

$$\frac{\partial h_\perp}{\partial t} = \lambda_\perp \frac{\partial h_\|}{\partial x}\frac{\partial h_\perp}{\partial x} + \Delta h_\perp + \eta_\perp(x,t). \tag{19b}$$

These are the most general equations which respect the symmetries of the problem. Non-linearities account for the variations of the local crack speed with the local orientation of the front. Galilean invariance leads to the result $\zeta_\| + z_\| = 2$.

If equation (19) is written directly as a 3d generalization of the KPZ equation, i.e. imposing the conditions that the crack velocity is contained in the plane defined by the force and the x-axis is parallel to the line (see figure 5), the term λ_x does not appear [46]. In this case, the numerical estimates of Ertaş and Kardar [30, 31] lead to

$$\zeta_\| \simeq 0.5 \qquad \zeta_\perp \simeq 0.72 \qquad z_\| = z_\perp \simeq 1.5. \tag{20}$$

When λ_x is equal to 0, $h_\perp$ disappears from equation (19*a*), which only concerns $h_\|$. In this case, the in-plane properties are decoupled from the out-of-plane ones (the reverse is not true), and it is expected that the in-plane properties of a purely three-dimensional front are the same as the properties of a front constrained to propagate within a plane. This seems

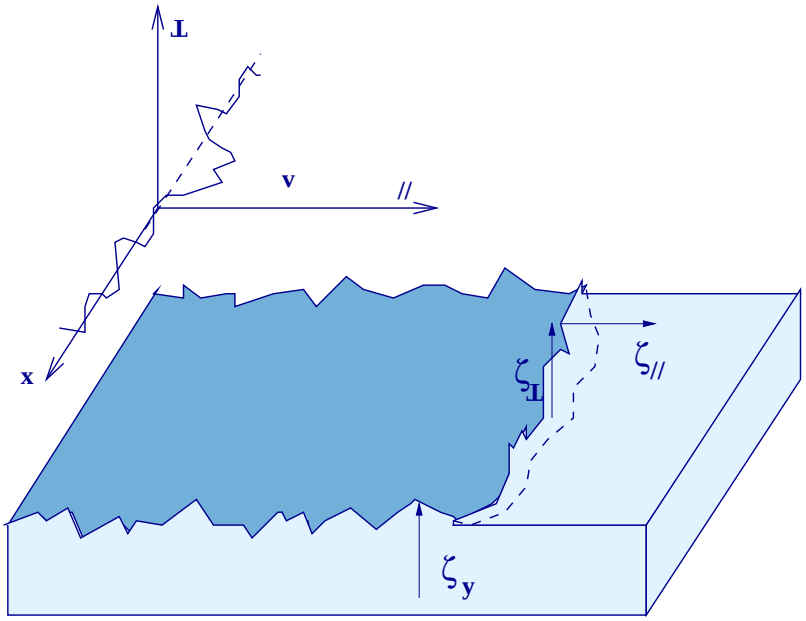

Figure 5. The definition of the various roughness indices which can be measured on a fracture surface: $\zeta_\perp$ is measured along profiles parallel to the x-axis (perpendicular to the direction y of crack propagation); $\zeta_\parallel$ is the in-plane roughness, i.e. the roughness of the projection of the crack front onto the plane xy of crack propagation; and ζ_y is the roughness measured on profiles lying along the direction y of crack propagation. If the crack propagates at a constant velocity, then one should have: $\zeta_y = \zeta_\perp / z_\perp$.

to indeed be the case experimentally [47, 48]. To our knowledge, this value of $\zeta_\perp$ is the only theoretical prediction reasonably close to the measured value, $\sim$0.8 (it will be shown in the next section that the most accurate experimental estimate [35] is 0.78).

Going back from this KPZ regime to the vicinity of the threshold, it can be shown that parallel and perpendicular perturbations do not propagate at the same rate:

$$z_\perp = z_\parallel + \frac{1}{\nu} \tag{21}$$

where ν has the definition given in equation (17), since the pinned domain has the same characteristic extension both parallel and perpendicular to the direction of line propagation. The argument given by Leshhorn *et al* [45] applies also in 3d, when considering the projection of the moving front onto the plane of propagation:

$$\beta = \nu(z_{\parallel,c} - \zeta_{\parallel,c}). \tag{22}$$

For a local line tension, it can be shown also that

$$\nu = \frac{1}{2 - \zeta_{\parallel,c}}. \tag{23}$$

In this case, isotropy further leads to

$$\zeta_{\parallel,c} = \zeta_{\perp,c} + \frac{1}{2} \tag{24}$$

which means that in the small-velocity regime—i.e. close to threshold, or at length scales smaller than ξ_c—the in-plane roughness index $\zeta_{\parallel,c}$ should be close to unity if $\zeta_{\perp,c}$ is close

to 1/2. It will be shown in the following that in fact both exponents are close to 1/2 in experiments [34, 35, 47].

In fact, neither equation (23) nor equation (24) hold if elastic long-range forces are taken into account. In particular, equation (24) becomes

$$\nu = \frac{1}{1-\zeta_{\|,c}}. \tag{25}$$

This should actually be the case for cracks, as first noticed by Gao and Rice [49] and by Schmittbuhl and co-workers [50]. These authors [50] built up a two-dimensional model using the non-local elastic kernel calculated to first order by Gao and Rice [49]. The structure of the non-local elastic term is the same as for the triple line in the problem of the wetting of a dirty surface. The numerical estimates of Schmittbuhl and co-workers [50] are very close to the renormalization group (RG) result obtained by Ertaş and Kardar in this case:

$$\zeta_c \simeq 0.35 \qquad z_c \simeq 1.5. \tag{26}$$

By studying a model rather close to the one of Schmittbuhl *et al* [50], Thomas and Paczuski [51] have obtained very different results, in agreement with a mean-field approach, leading to

$$\zeta_c = 1/2 \qquad \beta = 1 \qquad \nu = 2 \qquad z_c = 1. \tag{27}$$

The discrepancy between the two series of results does not seem to depend upon the nature of the forces, and already exists when short-range forces are taken into account. In fact, while Schmittbuhl *et al* consider forces higher than F_c and only allow—in a quasi-static way—the less pinned site to advance by a random length, Thomas and Paczuski consider the system below threshold, and allow local avalanches to occur, the size of which diverges when F is closer to F_c. This is reminiscent of the two models proposed by Sneppen [52], with short-range forces however. In both cases, the interface $z(x,t)$ is defined on a discrete chain $x = 1, \ldots, N$; also defined are a string of random Gaussian uncorrelated local pinning forces $\eta(x)$ constant over time (quenched disorder). As already noticed, the quenched or thermalized nature of the disorder is of particular importance when the crack velocity tends to zero. In the first model (model A in [52]), the site feeling the smallest pinning force is allowed to move by one unit under the condition that the local slope remains smaller than unity, i.e. $|z(x) + 1 - z(x \pm 1)| \leqslant 1$. The roughness exponent is then $\zeta = 1.00 \pm 0.01$, while β is also lying at around unity: $\beta = 0.95 \pm 0.05$.

In the second model considered by Sneppen [52] (model B), the constraint on the slopes acts *after* the least pinned site is moved. To fulfil this constraint, the neighbouring sites are compelled to advance as well, thus creating a local avalanche. This model leads to self-affine fronts characterized by a roughness $\zeta = 0.63 \pm 0.02$, and a β-exponent equal to 0.9 ± 0.1. The scaling theory of model B was proposed by Maslov and Paczuski [53].

On the other hand, on imposing a condition on the local curvature rather than on the slope, model A was studied numerically by Roux and Hansen [54]. In this case, the front is shown to be self-similar, with a roughness index greater than 1: $\zeta = 1.2$.

Hence it seems clear that the method used for approaching the threshold is crucial for the determination of the behaviour of the moving line. Whether one type of model or the other is more appropriate for fracture is still not clear at present.

Very recently, Ramanathan, Ertaş and Fisher considered a three-dimensional quasi-static non-local model [55]. Like in equation (19*a*), when $\lambda_x = 0$, in-plane properties are decoupled from out-of-plane ones, which seems to be the case experimentally [47, 48]. But, in complete disagreement with experiments, there is only one out-of-plane regime predicted,

Table 1. Comparison of the measured critical exponents with the predictions of the various 3d and 2d models of lines moving in random environments.

		Depinning transition	Moving phase
3d local model [30]	$\zeta_\perp$	0.5	0.72
	$\zeta_\parallel$	1.2	0.5
	$z_\perp$	2.3	1.5
	$z_\parallel$	1.3	1.5
	β	1	
	ν	1/3	
3d non-local model [55]		0.5 (mode III)	0.5 (mode III)
	$\zeta_\perp$	Logarithmic (mode I)	Logarithmic (mode I)
	$\zeta_\parallel$	1/3 (mode III)	Logarithmic (mode III)
	$z_\perp$		
	$z_\parallel$	7/9 (mode III)	
	β	7/9 (mode III)	
	ν	3/2 (mode III)	
2d local models	ζ	1 [52] model A, 0.63 [52] model B, [53], 1.2 [54]	1/2 [44]
	z		3/2 [44]
	β	1 [52] model A, 0.9 [52] model B	
	ν	2.8 [52] model B, [53]	
2d non-local models	ζ	1/3 [31], 0.35 [49], 0.5 [51]	Logarithmic
	z	7/9 [31]	
	β	7/9 [31], 1 [51]	
	ν	3/2 [31], 2 [51]	
Experiments	$\zeta_\perp$	0.5 [34–36]	0.78 [35], [1–19]
	$\zeta_\parallel$	0.54 [47], 0.55 [48]	
	$z_\perp$	2 [58]	1.2 [16]
	$z_\parallel$	1.5 [58]	
	β	2 [58]	
	ν	2 [58]	

independently of the crack velocity. Furthermore, $\zeta_\perp$ should be equal to 0.5 in the case of a mode III external loading, while the fracture surface should be only logarithmically rough under mode I loading. The residual stresses are found to be able to increase this roughness, but it appears likely to the authors that elastic wave propagation effects may be needed to explain the experimental observations. As will be seen in the following, the orders of magnitude of the measured crack speeds fail to suggest the relevance of inertial effects in the experiments. Even in the case of very discontinuous crack propagation modes, for which the measured velocity is in fact an average over too-large time-scales, one is indeed in the quasi-static regime. Ramanathan *et al* [55] also note that these models only consider uncorrelated noise, whereas the microstructural disorder might be strongly correlated at short length scales. This would only displace the problem, since the new question would concern universality of internal stress correlations in materials. On the other hand, non-linearities which are shown to be irrelevant to first order might be important. More generally, the high local slopes observed on the fracture surfaces of metallic materials might lead one to question the relevance of perturbative theories.

Finally, table 1 summarizes the results obtained using the models quoted, compared to experimental measurements.

Act IV—experiments and simulations: two regimes of fracture—from 'quasi-static' to 'rapid'?

It is very tempting to use these theoretical models in order to give a unified interpretation of the various series of experiments at different length scales, or at different crack velocities. On the other hand, this theoretical framework suggests that on very general grounds, for each regime (close to threshold and beyond threshold), a fracture surface is characterized by three *a priori* independent roughness indices (see figure 5). As will be shown in this section, most of these exponents have now been measured experimentally.

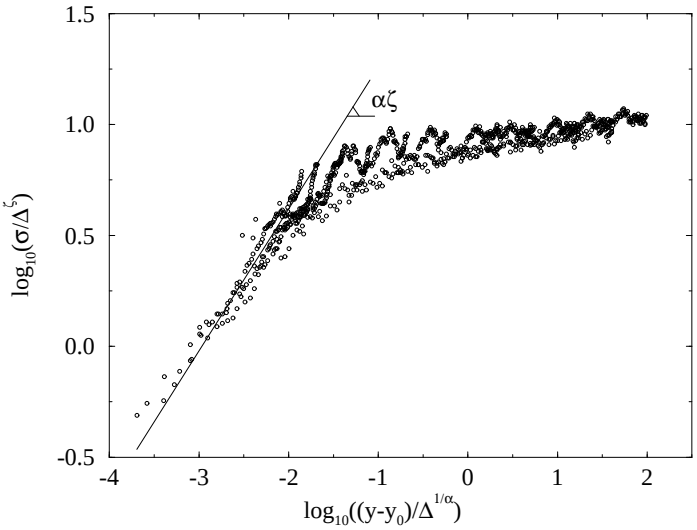

Figure 6. (Courtesy of J Schmittbuhl [16].) $\sigma(\Delta)/\Delta^{\zeta}$ is plotted on a log–log diagram as a function of $(y - y_0)/\Delta^{1/\alpha}$ for 100 profiles perpendicular to the direction of crack propagation. $y - y_0$ is the distance from the profile considered to the initial notch, Δ is a distance along the x-axis (perpendicular to the direction y of crack propagation), and $\sigma = \langle (z(r+\Delta) - z(r))^2 \rangle_r^{1/2}$.

Scene 1. Roughness of the front along the direction of crack propagation

Schmittbuhl and co-workers [57] have characterized the out-of-plane scaling properties of a granite fracture surface (see figure 1(e)) along the direction of crack propagation (see figure 4). For that purpose, they have examined one hundred profiles perpendicular to that direction, lying at various distances y from the initial straight notch. They have shown that the evolution of the self-affine correlation length $\xi_\perp$ (the upper limit of the '0.8' regime) from a 'microscopic' size typical of the initial straight notch was following a power law:

$$\xi_\perp \propto y^{\alpha} \qquad \alpha \simeq \frac{1}{1.2}. \tag{28}$$

The rescaling of all one hundred profiles over one master curve is shown in figure 6.

It would be tempting to interpret the exponent α as $1/z_\perp$ within the framework of the models quoted in the previous section (Act III), and to compare the experimental result with the prediction of the Ertaş–Kardar model $z_\parallel = z_\perp \simeq 1.5$ (see equation (20)). However, this comparison would be relevant if the experiments of Schmittbuhl *et al* had been performed at a constant velocity during crack propagation. In that case, y would have

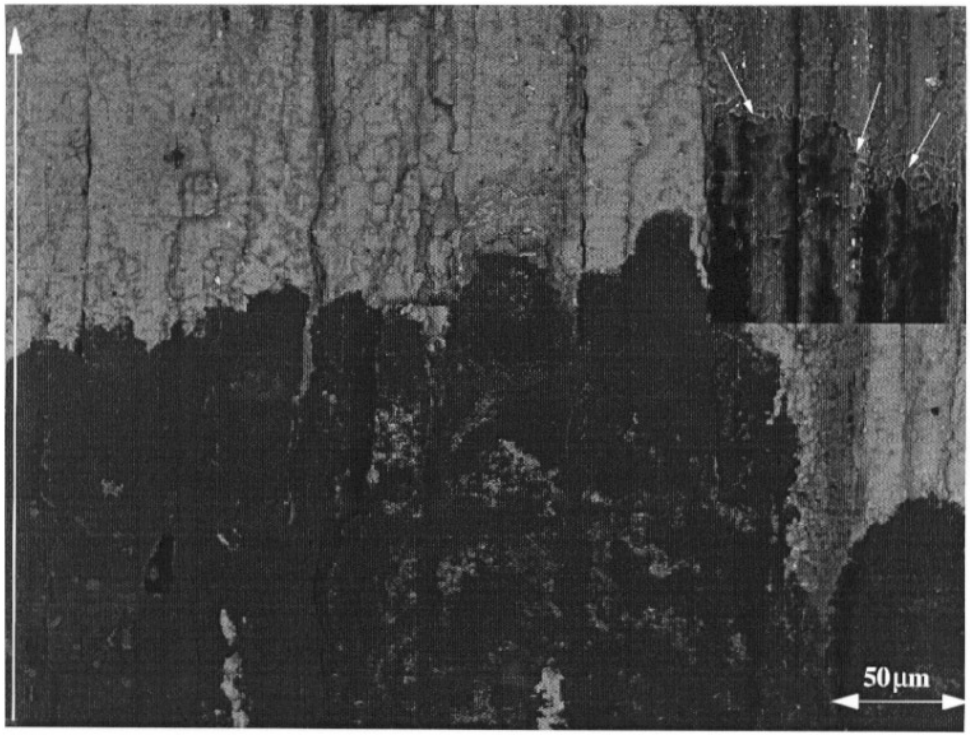

Figure 7. A fracture front marked with indian ink in the 8090 aluminium alloy, observed with a SEM (backscattered-electron contrast). The white arrow on the left indicates the direction of crack propagation (parallel to the length of the very elongated metallurgical grains). Inset: a fracture front marked with indian ink, observed with a mixed signal (secondary + backscattered electrons) exhibiting characteristic dimples (indicated by white arrows).

indeed corresponded to time. Since fracture was obtained by throwing a knife into the initial notch, this is very unlikely.

Scene 2. In-plane roughness of arrested crack fronts

In-plane exponents—$\zeta_{\parallel,c}$ and $\zeta_{\parallel}$—have received less attention from experimentalists. In fact, these exponents are more difficult to reach. In the 'moving phase', in particular, $\zeta_{\parallel}$ should be measured *during* propagation. It seems that such an experiment would be possible only by registering the crack front evolution with a camera in a transparent material. In contrast, $\zeta_{\parallel,c}$, characterizing the 'pinned' phase, could be measured from the observation of marked arrested cracks in two different metallic alloys [47, 36].

To do this, fracture was arrested during propagation either in tension (on a 8090 aluminium–lithium alloy), or in fatigue (for the Ti_3Al-based Superα_2 [56]), and indian ink was injected into the cracks under a moderate vacuum. The samples were subsequently carefully dried, and fracture was completed. It could be checked in each case that the limit of indian-ink-covered metal did indeed correspond to arrested crack fronts (see figure 7). In both cases, these fronts could be observed over three decades of length scales. In the case of the Superα_2, it was found that

$$\zeta_{\parallel,c} \simeq 0.54 \tag{29}$$

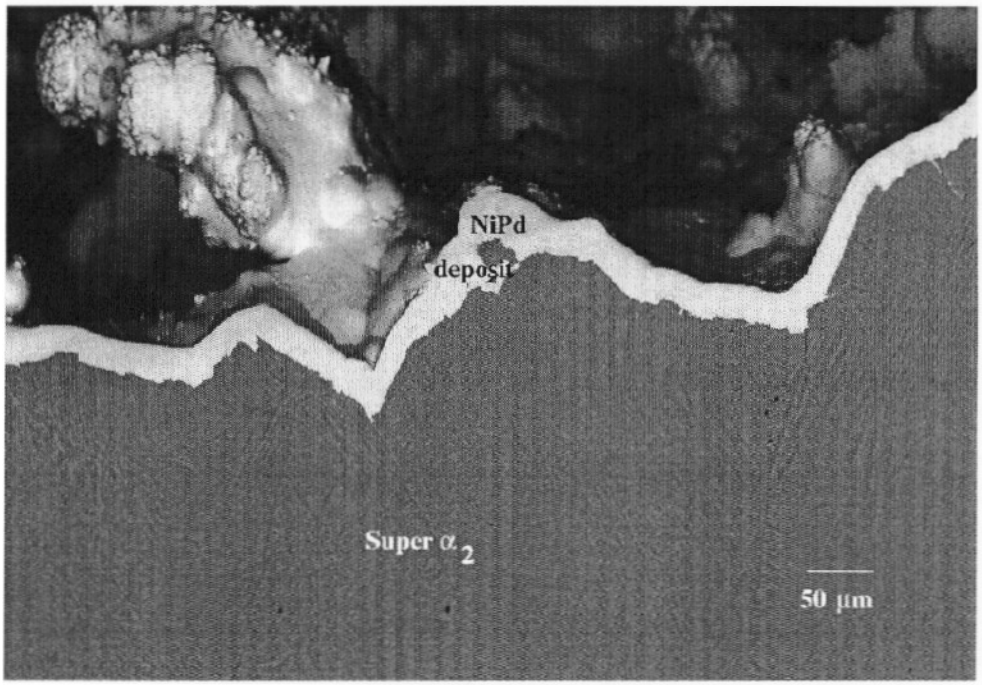

Figure 8. A fracture front (perpendicular to the direction of crack propagation) in the Superα_2. The fracture surface is plated with NiPd. The deposit appears in very light grey above the alloy where the needles of α_2-phase are visible.

while a result closer to $\zeta_{\parallel,c} \simeq 0.6$ was found in the case of the 8090 aluminium alloy. Although the two results are clearly compatible with one another, it was suggested that the slight difference could be due to the highly anisotropic microstructure of the Al–Li material. In fact, fracture was propagating in the direction of very elongated metallurgical grains (length 0.3 mm $\times$ width 100 μm $\times$ thickness 20–50 μm; see figure 7, showing that grain boundaries seem to be efficient pinning sites in that case, although there are some others at smaller length scales).

Scene 3. Perpendicular exponents: two regimes

To provide a clear experimental answer to the question of whether or not there are two regimes of fracture (in the vicinity of the depinning transition, and in the moving phase), crack fronts were analysed at different velocities. In the first experiments, performed on the Superα_2, the crack velocities could not be measured, but various profiles perpendicular to the direction of crack propagation were analysed along a chevron-notched CT sample (see figure 2(a)) precracked in fatigue and broken in tension. The microstructure of the Superα_2 [56] mainly consists of brittle α_2 laths of various sizes (average: 1 μm in diameter $\times$ 10 μm in length, but much finer needles are present also), arranged in colonies of parallel needles (average width: 50–70 μm) with various orientations, immersed in a more ductile β-phase (grain size: $\sim$1 mm). The volume fractions of the two phases are comparable in the experiments considered.

In the first series of experiments, profiles obtained from fatigue fracture (tension–tension)

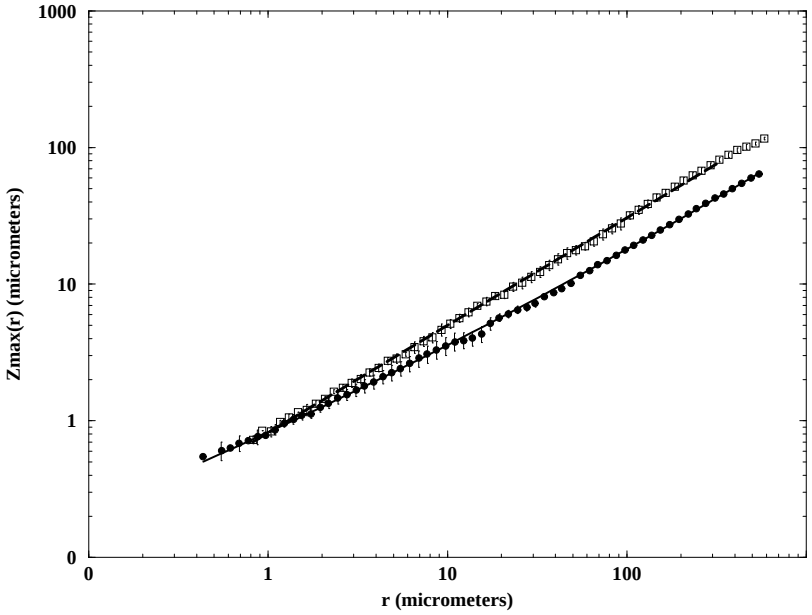

Figure 9. $z_{max}(r)$ plotted versus r on a log–log plot: □, fracture in tension; also shown is a fit (dashed line) with a single power law with exponent 0.78. •: with fracture in fatigue; in this case the fit is the sum of two power laws with exponents 0.5 and 0.78 (solid line; $\xi_c \simeq 5$ μm). Error bars account for the dispersion of the results for the various micrographs analysed. Note that the small-length-scales regimes coincide.

were compared to profiles corresponding to tensile fracture on the same sample. Fifteen micrographs at various magnifications ($\times 50$ to $\times 5000$) were studied along one profile lying in the fatigue fracture zone where the average crack velocity was known to be particularly low (the maximum load was drastically decreased to avoid complete failure of the specimen before the tensile test was started), and fifteen micrographs corresponding to a tensile fracture profile close to the edge of the sample were considered as well (see an example in figure 8). In the latter case, it was possible to fit the evolution of $z_{max}(r)$ (equation (5)) with a single power law with exponent 0.78 over approximately three decades of length scales (figure 9). In the former one, however, this was impossible, and the existence of a small-length-scales regime characterized by an exponent close to 0.5 (extending up to a crossover length of $\simeq 5$ μm) was clearly shown (see figure 9).

In order to investigate better the small-length-scales regime, and to compare tensile fracture fronts propagated at different velocities, further experiments on the Superα_2 were performed using simultaneously an AFM, in collaboration with F Creuzet and S Hénaux [35], and a standard SEM. For that purpose, one fracture surface of a CT sample was plated with NiPd, and subsequently cut, polished, and observed with a SEM at various magnifications in order to characterize two tensile fracture profiles, one being close to the fatigue fracture zone, and the other one to the edge of the specimen. On the opposite fracture surface, ten AFM records were registered along the same profiles. For each SEM or AFM record, several statistical quantities were computed: z_{max} (equation (5)), P_0 (equation (4)), and the power spectrum $S(q)$, which were shown to provide comparable results. Furthermore, the results obtained from the AFM records were shown to be compatible with those obtained

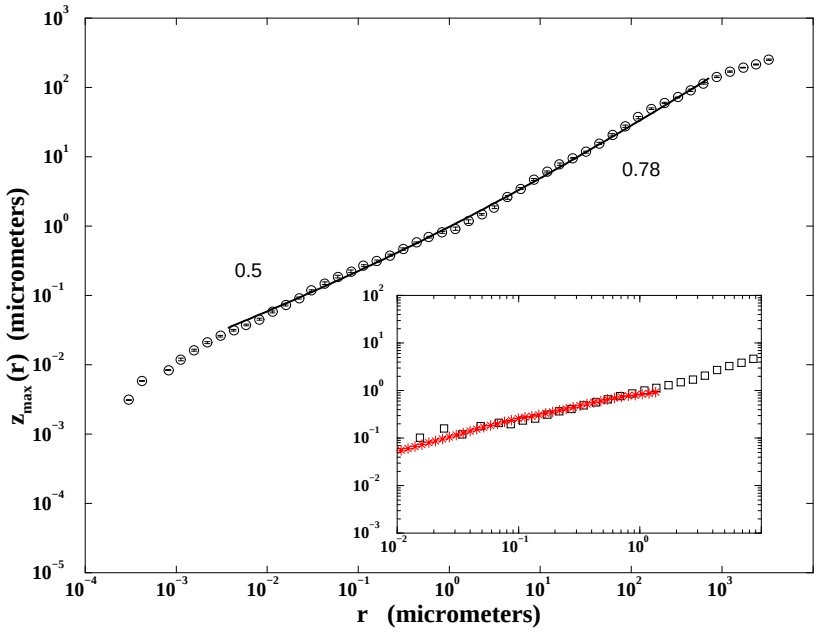

Figure 10. The region close to the fatigue fracture zone. $z_{max}(r)$ is plotted versus r on a log–log plot. Note that the experimental points obtained with the two techniques gently collapse onto the same curve (the region of overlap of the two techniques extending approximately from 10 nm to 1 μm). The fit simply corresponds to the sum of two power laws with exponents 0.5 and 0.78: $z_{max}(r) \propto (r/\xi_c)^{0.5} + (r/\xi_c)^{0.78}$, with $\xi_c = 0.1$ μm. The error bars are estimated from the scattering of experimental results relating to the various micrographs or profiles analysed. Inset: the region of overlap between the AFM ($\star$) and SEM ($\Box$).

from the SEM observations, overlapping over two decades of length scales (approximately from 10^{-2} to 1 μm; see figure 10), when the conversion factor of the AFM is chosen to match the SEM one. For the profile closer to the edge of the specimen, it was shown that a single power law with exponent $\zeta = 0.78$ could fit the data *over five decades of length scales* (from 5 nm to 0.5 mm; see figure 11). In contrast, when considering the profile close to the fatigue fracture zone, two power laws were needed (see figure 10), with the following exponents: $\zeta \simeq 0.78$ at large length scales (0.1 μm–1 mm) and $\zeta_c \simeq 0.5$ at smaller ones (5 nm–0.1 μm).

Since these two profiles were corresponding to two different stress intensity factors K_I and crack velocities v, these results were in qualitative agreement with the above models: they have proved the existence of two fracture regimes characterized by significantly different roughness exponents (0.5 and 0.78), crossing over to one another at a length scale depending upon K_I or v. Nevertheless, measurements of the average crack velocity v during tensile fracture proved impossible with the available experimental apparatus, and it was decided to perform more quantitative experiments in fatigue fracture, where a propagating crack can be more easily slowed down than in pure tension.

Before going on to the description of these more quantitative experiments, let us quote new large-scale MD simulations [37, 38] concerned with the morphology of fracture surfaces of amorphous materials, which are in remarkable agreement with experimental results. In fact, it is found that, as far as profiles perpendicular to the direction of crack propagation are concerned, there are two self-affine regimes with roughness exponents $\zeta_{\perp,c} \simeq 0.5$ at small

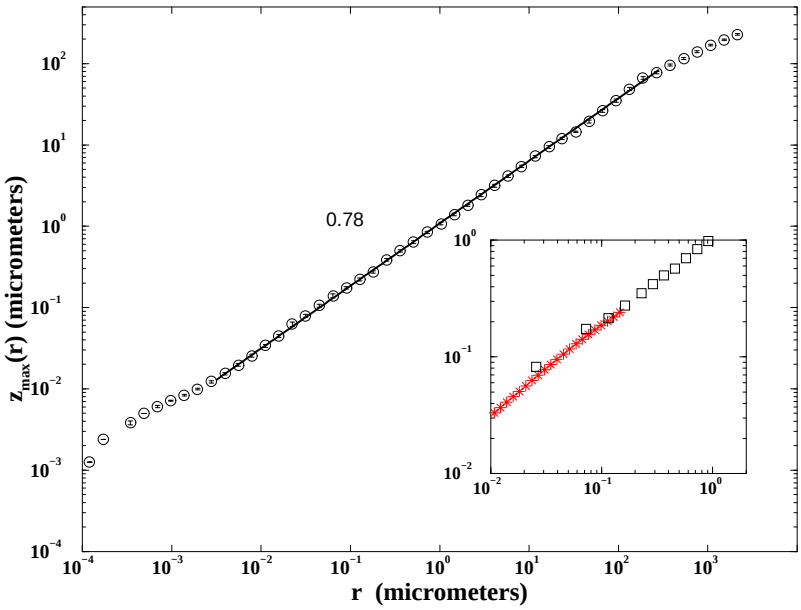

Figure 11. The region close to the edge of the specimen. $z_{max}(r)$ is plotted versus r on a log–log plot. The best fit of the data is a single power law with exponent 0.78: $z_{max}(r) \propto r^{0.78}$. Note that the 'rapid-fracture' regime extends over approximately *five* decades of length scales: 5 nm–0.5 mm. Inset: the region of overlap between the AFM (⋆) and SEM (□).

length scales and $\zeta_\perp \simeq 0.8$ at larger ones, while the 'large'-length-scales exponent measured along the direction of crack propagation is close to 0.7, i.e. in good agreement with the result obtained by Schmittbuhl *et al*. Samples of 100 Å^3 (corresponding approximately to 10^6 atoms!) are considered in these simulations. The simulated crack velocities however are much larger than the experimental ones (see below—the experiments on a silicate glass), and rather close to the Rayleigh wave speed. The crossover lengths are also far smaller. Nevertheless, not only do the exponents perfectly correspond to the experimentally measured ones, but the crossover function is very close too: as will be shown below, this crossover is much more abrupt for amorphous materials than for the Superα_2. Finally, although active at very different length scales, the fracture modes seem to be the same as for the Superα_2: cleavage at small length scales, followed by cavity coalescence with the crack tip. For the Superα_2, cleavage occurs within the α_2 needles. These microcracks are grown into cavities which are blunted at their passage into the β-phase. Further crack progression occurs by coalescence of these cavities with the main crack tip. A qualitative comparison of what is observed *in situ* with a SEM to what is obtained with MD simulations (see figure 12) is quite striking!

Scene 4. Perpendicular exponents: depinning of crack fronts

The most recent experiments concern the vicinity of the 'depinning transition', studied on two drastically different materials: the Superα_2 and a soda-lime silica glass [58].

Two notched CT specimens of Superα_2 were broken in fatigue. Fatigue tests were carried out using an electro-servohydraulic testing machine, operating under load control. The tests were performed in air with a constant stress ratio $R = \sigma_{min}/\sigma_{max} = 0.1$ (σ_{max} and

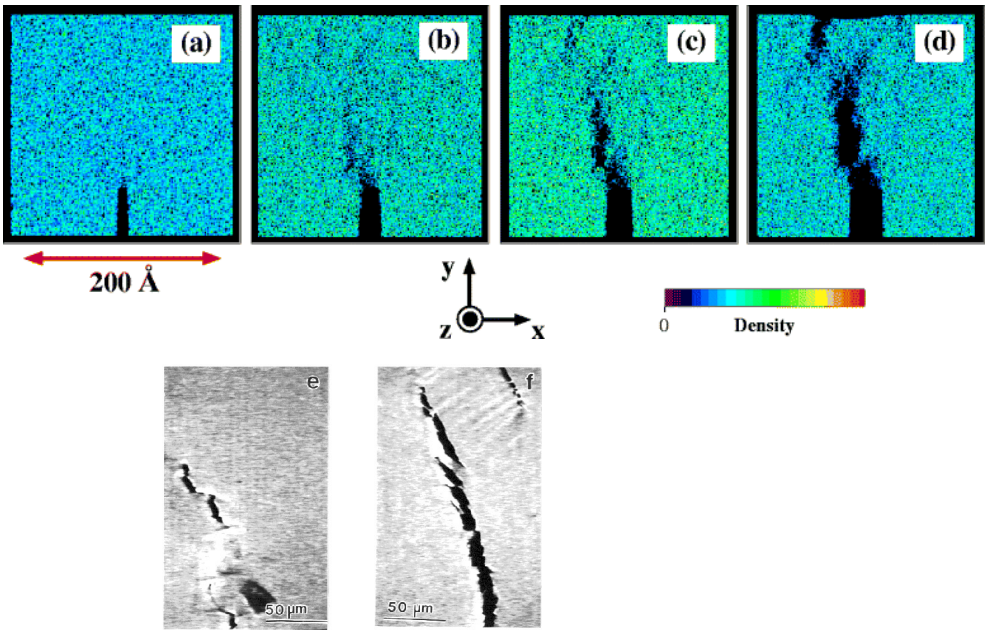

Figure 12. (a) to (d): results of MD simulations on the fracture of amorphous materials on the scale of 100 Å (courtesy of R Kalia, A Nakano and P Vashishta [38]). (e) and (f): SEM *in situ* observations: crack propagation in tension in small CT samples of Superα_2 first precracked in fatigue.

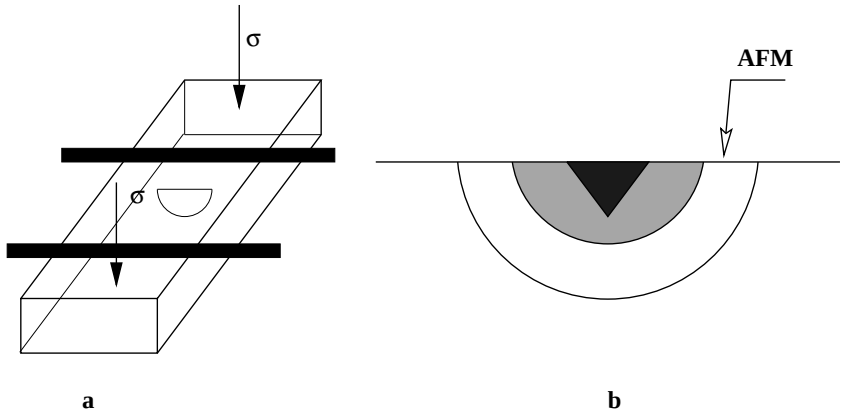

Figure 13. (Courtesy of B Nghiem and F Creuzet.) (a) The experimental four-points bending system. (b) A sketch of the indented plate of glass. The zone in which the AFM observations are performed is indicated by an arrow.

σ_{min} are respectively the minimum and the maximum stresses), at a frequency $f = 30$ Hz. The evolution of the crack length a with time was measured using the potential-drop method [61]. The fracture surfaces were observed for four different velocities spanning from 10^{-9} to 10^{-6} m s^{-1}, using both an AFM and a SEM.

Fracture surfaces of soda-lime silica glass have been prepared by controlling the crack propagation with a four-points bending system (see figure 13). After the initial propagation,

which allows one to relax all residual stresses, the plate was properly loaded in order to obtain the required average crack velocity. This velocity was measured by imaging the crack tip with an AFM at different times [18]. The humidity rate was measured, and kept between 37 and 41%. The controlled crack propagation is maintained over a distance of about 30 μm, so that fracture surfaces can be easily probed with an AFM. The crack velocities range from 2×10^{-9} to 10^{-7} m s^{-1}. Ten AFM height profiles of length 1.5 μm were registered perpendicularly to the direction of crack propagation ($\perp$) on three samples, and along this direction ($\parallel$) for four other specimens, in the mirror zone (see figures 1(a) and 1(b)). As will be shown in the following, no significant anisotropy could be detected.

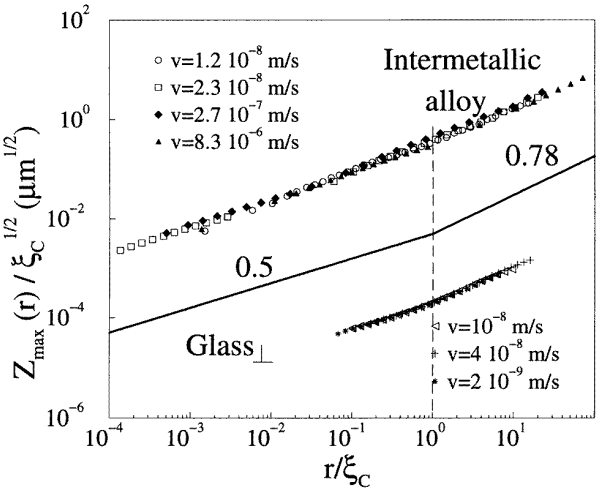

Figure 14. (See reference [58].) $z_{max}(r)/\sqrt{\xi_c}$ is plotted against r/ξ_c for the two materials separately. Note that in these reduced units, the plots corresponding to the various velocities collapse onto the same curve. Although the crossover regions are quite different for the two materials, the asymptotic regimes are well described by power laws with exponents 0.5 ($r/\xi_c \ll 1$) and 0.78 ($r/\xi_c \gg 1$).

In order to determine the roughness exponents ζ_c, ζ, and the crossover length ξ_c of the profiles analysed, the quantity $z_{max}(r)$ was computed for each record, and averaged for each profile. For the Superα_2, over the whole range of observations, $z_{max}(r)$ is very well fitted by the sum of two power laws: $z_{max}(r) = A((r/\xi_c)^{0.5} + (r/\xi_c)^{0.78})$. The small- and large-length-scales roughness indices—0.5 and 0.78 respectively—are chosen to fit with the results of previous experiments [35]. As already mentioned when considering the results of MD simulations, the crossover between the two regimes is much sharper in the case of glass, and, in this case, the crossover length ξ_c was determined as the intersection of the two asymptotic power-law regimes with exponents 0.5 and 0.78. Once the crossover lengths have been determined in each case, it is possible to plot z_{max} as a function of r/ξ_c. In figure 14, curves showing $z_{max}(r)/\sqrt{\xi_c}$ for each material are plotted as functions of r/ξ_c, and shown to collapse onto the same master curve. In both cases, the asymptotic regimes are well described by power laws with exponents 0.5 at small length scales ($r/\xi_c \ll 1$), and 0.78 at large length scales ($r/\xi_c \gg 1$). In other words, one can write

$$z_{max}(r) \simeq r^{0.5} f\left(\frac{r}{\xi_c}\right) \tag{30}$$

with $f(x \to 0) \sim 1$ and $f(x \gg 1) \sim x^{0.28}$, showing that the amplitude of the small-length-scales contribution is independent of ξ_c, and hence of crack velocity.

These results, obtained for materials as different as an intermetallic alloy and a glass, confirm previous observations [35, 34], where the short- and large-length-scales regimes were interpreted, respectively, as a 'quasi-static' and a 'rapid' regime.

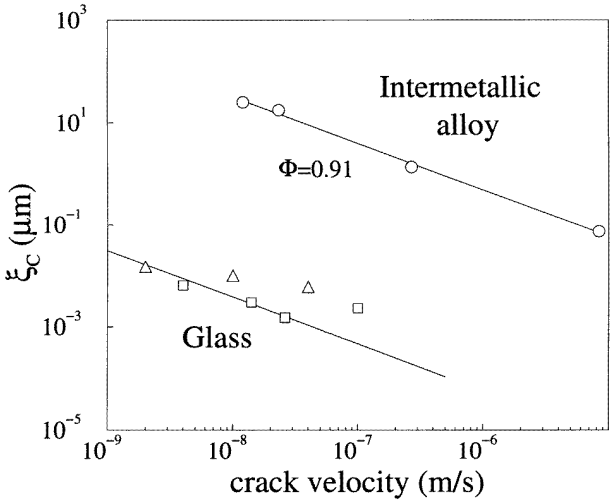

Figure 15. (See [58].) The evolution of the crossover length ξ_c with the crack velocity for the Superα_2 (○) and for soda-lime silica glass (△/□: perpendicular (⊥)/parallel (∥) to the direction of crack propagation). ξ_c is plotted versus v on a log–log plot, exhibiting a power-law dependence with an exponent $\phi \simeq 0.91$.

As can be seen in figure 15, ξ_c decreases with the crack velocity v in both cases, although the measured values of ξ_c are approximately 1000 times larger in the case of the Superα_2 than in the case of glass. In that respect, these experimental results can be interpreted as being a consequence of the small-scale heterogeneity of glass [59, 60]. They are compatible with a power-law decrease $v^{-\phi}$ in both cases, with an estimated value of ϕ close to unity. Note that the values of ξ_c measured for glass for the higher velocities might be overestimated: in this case the precision is very bad, since ξ_c is of the order of some nanometres, i.e. close to the resolution limit of the AFM.

In figure 16, both ξ_c and v for Superα_2 are plotted against the stress intensity factor $\Delta K = (\sigma_{max} - \sigma_{min})\sqrt{a}$. The fatigue crack growth in this regime is widely known as being intermittent [62, 63]. In this regime, the crack tip opens and closes many times before it can extend over a small distance. This process is repeated several times and causes incremental crack advance. The number of cycles required to get the crack to advance decreases as ΔK increases, and the crack motion is more and more continuous, microstructural obstacles being efficient at smaller length scales. At a given time, the force F exerted on the fracture front is proportional to ΔK, while the threshold force F_c is proportional to ΔK_{Th} (defined in figure 16). As the frequency of oscillation of these forces is far more rapid than the crack propagation, only the average force needs to be considered, which legitimates the analogy with the above-quoted models. In the case of glass, F is proportional to the stress intensity factor K, while F_c is proportional to the threshold K_{Th}. Preliminary results indicate that, in the sub-critical regime, the crack velocity is not uniform, and intermittency is likely to occur. Thus, in both cases, the pinning/depinning scenario is qualitatively satisfactory.

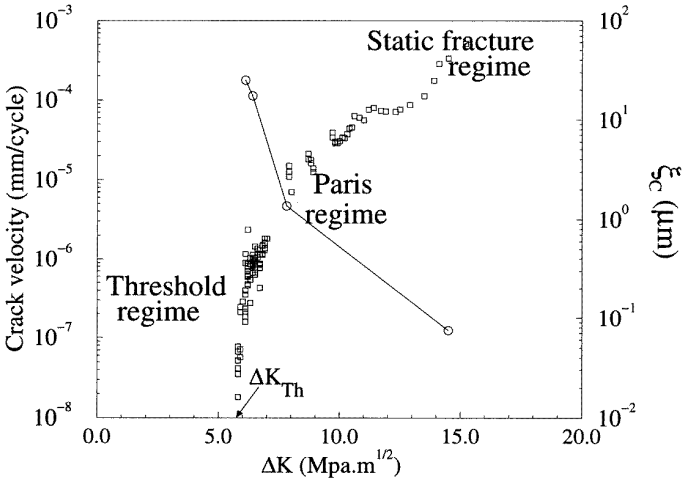

Figure 16. (See [58].) Superα_2: the fatigue crack velocity (□) as well as the crossover length ξ_c (○) are plotted against the stress intensity factor ΔK. The threshold value ΔK_{Th} is indicated.

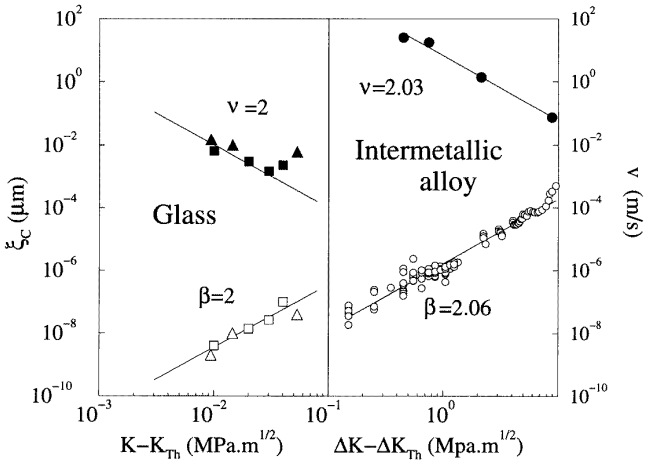

Figure 17. (See [58].) Superα_2 (○): the fatigue crack velocity (white symbols) is plotted versus $\Delta K - \Delta K_{Th}$ on a log–log plot, as well as the crossover length ξ_c (black symbols). Glass (△/□: perpendicular (⊥)/parallel (∥) to the direction of crack propagation): the crack velocity is plotted as a function of $K - K_{Th}$ (white symbols), as well as ξ_c (black symbols).

Figure 17 shows the evolution of the crack velocity v as a function of $\Delta K - \Delta K_{Th}$ for the Superα_2 and as a function of $K - K_{Th}$ for glass. In the case of the Superα_2, experimental measurements reveal a power-law increase without any change between the so-called 'threshold' and Paris regimes [63] (figure 16). In contrast, when static fracture occurs, a clear deviation from the power law can be observed for high values of $\Delta K - \Delta K_{Th}$. A fit of these data gives $\beta \simeq 2$. This value is compatible with the measurements on glass (figure 17).

In figure 17, ξ_c is plotted, also for both materials. A power-law decrease can be

observed, and the fit of the data relating to the metal gives $\nu \simeq 2.06$, compatible with the results on glass.

One can note that $\phi = \nu/\beta \simeq 1$. On the other hand, it is expected that the exponent n characterizing the range of interactions ($n = 2$ for local models—see reference [27] and equation (23)—and $n = 1$ for models taking into account the non-locality of elasticity—see reference [32] and equation (25)) is related to the exponents ν and $\zeta_\parallel$ through the relation

$$n = \zeta_\parallel + \frac{1}{\nu}. \tag{31}$$

If $\zeta_\parallel$ is taken equal to 0.54 [47] (equation (29)), this leads to a value of $n \simeq 1.03$, very close to unity, as expected for elastic interactions [32, 50, 51] (equation (25)). The 2d model of Thomas and Paczuski [51] (see table 1) gives results rather close to the experimental estimates of $\zeta_\parallel$ and ν: $\zeta = 0.5$ and $\nu = 2$, but the value of β is quite different, since they find $\beta = 1$.

Using equations (21) and (22), one can in principle deduce from the estimates of β, ν, and $\zeta_\parallel$ the values of the dynamic exponents: $z_\parallel \simeq 1.5$ and $z_\perp \simeq 2$. Hence, perturbations on the crack front are diffusive perpendicularly to the direction of crack propagation, while they are slightly hyper-diffusive along this direction.

For ductile materials such as Superα_2, the plastic zone size R_{plast} should be a relevant length scale as well. Although the same regimes are observed over the whole range of ΔKs, it can be noted that R_{plast} exceeds ξ_c for the two experiments corresponding to higher velocities, i.e. within the Paris regime. In the case of glass, the plastic zone size has been estimated also [18] to be of the order of some nanometres, i.e. of the order of magnitude of ξ_c.

The question of plasticity is in fact very striking on more general grounds, since no experiment, to our knowledge, indicates a crossover to a new regime when the plastic zone size is exceeded. One possible answer is that the exponent characterizing the fracture surface within that zone could be very close to ζ_c or ζ, so no new regime can be properly characterized. In fact, Roux and Hansen and co-workers have suggested [64, 65] that for perfect plasticity, the fracture surface should be a 'minimum-energy surface' [66–68], i.e. the surface for which the energy *globally* spent during the fracture process is a minimum. This is obviously a quasi-static assumption, since fracture is an irreversible process, for which the system cannot wander to the lower-energy state. Recent estimates of the roughness indices of minimum-energy surfaces led to [68–70]

$$\zeta_{M.E.S.} \simeq 0.45 \tag{32}$$

which is close enough to the measured value of ζ_c to be confused with it. One possible scenario that one could think of is the following. At low enough ΔK, in fatigue experiments, the plastic zone size R_{plast} is much smaller than ξ_c, and the roughness index is $\zeta_{M.E.S.}$ up to distances of the order of R_{plast}, and ζ_c for length scales intermediate between R_{plast} and ξ_c, although no crossover can be detected experimentally, the two exponents being too close to one another and/or R_{plast} being too close to the resolution limit of the AFM. Outside the plastic zone, perfect elasticity can in fact be assumed, and the pinning/depinning scenario with non-local elasticity described above is likely to occur. Hence, for low enough ΔK, ξ_c should decrease with the crack velocity. In contrast, when ΔK is increased, R_{plast} increases also, and there should exist a value $\Delta K^\star$ above which R_{plast} becomes greater than ξ_c. In this case, the 'pinning/depinning' scenario is no longer valid, and what is observed is the plastic regime characterized by $\zeta_{M.E.S.}$, up to R_{plast}, while at larger length scales, the '0.8' regime can be expected again. This assumption, however, requires that the observed crossover between the small- and large-length-scales regimes takes place at

R_{plast} for $\Delta K > \Delta K^{\star}$. Since classical theories predict an increase of R_{plast} with ΔK, one should observe an increase of the crossover length with ΔK when $\Delta K > \Delta K^{\star}$. As shown previously, this does not seem to be the case experimentally, but one cannot exclude the possibility that this occurs for higher values of ΔK and v.

Act V—pinning/depinning: that is the question

Twelve years of quantitative analysis have shown that the morphology of fracture surfaces is rich enough to help us to achieve more of an understanding of crack propagation in heterogeneous materials. Their scaling properties have now been extensively studied, and shown to extend sometimes over five decades of length scales, which makes them among the best-characterized scaling phenomena in natural sciences.

It has been argued that the 'large-length-scales/high-velocities' roughness index is universal. Non-significant differences in the measured exponents may arise from differences in length scales. It is indeed clear that the correlation length ξ, for example, is strongly material dependent: the same scaling properties are observed for metallic materials up to length scales of the order of 1 mm, while they hardly extend beyond $\sim$100 nm for glass, both in the mirror and the mist zones [71]. In fact, ξ seems to be of the order of the largest heterogeneity in the material considered. On the other hand, it appears quite clearly now that there is another self-affine regime at smaller length scales/smaller velocities. When observations are possible over only two decades of length scales, a power law with an effective exponent, intermediate between the two values 0.5 and 0.8—depending on the proportions of the two regimes which are accessible—can perfectly fit the data.

The very existence of these two regimes is close to the predictions of models of lines moving in random environments, the relevance of which to fracture has been suggested in [33]. Obviously, these models are not yet suitable for fracture, but some of their conclusions help in a synthetic reading of complex experimental results.

Among the weaknesses of the existing approaches—usually not meant to describe crack propagation—Schmittbuhl and co-workers [50] have noticed the importance of non-locality of elasticity [49]. An attempt to take these into account in three dimensions has been performed in [55]. Although it fails to predict the experimental observations, this model is particularly interesting, and could be modified without taking into account inertial effects.

On the other hand, the quasi-static assumption might be wrong, if inertial effects are indeed relevant on a very local scale. Experiments and models concerned with truly dynamic fracture [72–76] have not been quoted here—except MD simulations—although they might be relevant to an understanding of the observations. As most experiments in dynamic fracture are performed on glass or on polymeric materials, in the domain where they are in fact homogeneous, we have long considered that the two situations (quasi-static and dynamic) could be separated—until more was understood, like, say, turbulence as compared to laminar flow in porous media! This might be a completely wrong picture, however [77], and more should be known soon.

For amorphous materials, MD simulations are particularly promising. They might be very efficient as regards the understanding of fracture, allowing for the analysis of the entire stress distribution in the material during crack propagation. They are particularly well adapted to dynamic fracture, since the crack velocities are close to the Rayleigh speed. It might not be possible to reach low velocities with these simulations, because they are still computer time consuming. Strikingly, however, the morphologies of the fracture surfaces generated by this technique are very close to those observed experimentally in the 'quasi-static' regime.

The scenario predicted by the line-moving models is very close to what is observed for real materials. Some other phenomena might arise when the stress intensity factor is such that plasticity cannot be neglected any longer, and this will be analysed in further experiments on more ductile aluminium alloys.

Finally, more macroscopic calculations could use as a basic element the results of these 'microscopic' models in order to predict the mechanical behaviour of complex materials.

As a conclusion, a great deal of work has been achieved in the field of 'fracture seen by statistical physicists', and yet a lot still remains to be done for a clear image to appear.

Acknowledgments

I am very much indebted to all of my collaborators, starring: J-P Bouchaud, F Creuzet, P Daguier, S Hénaux, G Lapasset, G Marcon, S Navéos, B Nghiem, E Orignac, and J Planès. Fruitful discussions with D Ertaş, D Fisher, R Kalia, B Mandelbrot, A Nakano, J Rice, S Roux, J Schmittbuhl, V Silberschmidt, and P Vashishta are gratefully acknowledged as well. Many thanks also to P Beauchêne, J-M Dorvaux, and C Grisot for their valuable help, and to F Creuzet, R Kalia, and J Schmittbuhl for allowing me to reproduce some of their figures.

References

[1] Mandelbrot B B, Passoja D E and Paullay A J 1984 *Nature* **308** 721
[2] Mandelbrot B B 1985 *Phys. Scr.* **32** 257
[3] Isichenko M B 1992 *Rev. Mod. Phys.* **64** 961
[4] Feder J 1988 *Fractals* (New York: Plenum)
[5] Mu Z Q and Lung C W 1988 *J. Phys. D: Appl. Phys.* **21** 848
[6] Dauskardt R H, Haubensak F and Ritchie R O 1990 *Acta Metall. Mater.* **38** 143
[7] Mecholsky J J, Passoja D E and Feinberg-Ringel K S 1989 *J. Am. Ceram. Soc.* **72** 60
[8] Mecholsky J J, Mackin T J and Passoja D E 1988 *Adv. Ceram.* **22** 127
[9] Tsai Y L and Mecholsky J J 1991 *J. Mater. Res.* **6** 1248
[10] Bouchaud E, Lapasset G and Planès J 1990 *Europhys. Lett.* **13** 73
[11] Bouchaud E 1996 Size-scale effects in the failure mechanisms of materials and structures *IUTAM Symp. (Turin, 1994)* ed A Carpinteri (London: Spon) p 121
[12] Måly K J, Hansen A, Hinrichsen E L and Roux S 1992 *Phys. Rev. Lett.* **68** 213
[13] Lemaire E, Ould Mohamed Abdelhaye Y, Larue J, Benoit R, Levitz P and Van Damme H 1993 *Fractals* **1** 968
[14] Bouchaud E, Lapasset G, Planès J and Navéos S 1993 *Phys. Rev.* B **48** 2917
Planès J, Bouchaud E and Lapasset G 1993 *Fractals* **1** 1059
[15] Schmittbuhl J, Gentier S and Roux S 1993 *Geophys. Res. Lett.* **20** 8
Schmittbuhl J, Gentier S and Roux S 1993 *Geophys. Res. Lett.* **20** 639
[16] Schmittbuhl J, Roux S and Berthaud Y 1994 *Europhys. Lett.* **28** 585
[17] Imre A, Pajkossy T and Nyikos L 1992 *Acta Metall. Mater.* **40** 1819
[18] Guilloteau E, Charrue H and Creuzet F 1996 *Europhys. Lett.* **34** 549
[19] Guilloteau E, Arribart H and Creuzet F 1996 *Fracture-Instability Dynamics, Scaling, and Ductile/Brittle Behavior; MRS Fall Meeting (Boston, MA, 1995)* vol 409, ed R L Blumberg-Selinger, J J Mecholsky, A E Carlsson and E R Fuller (Pittsburgh, PA: MRS) p 343
[20] Bouchaud E and Bouchaud J-P 1994 *Phys. Rev.* B **50** 17 752
[21] Milman V Y, Blumenfeld R, Stelmashenko N A and Ball R C 1993 *Phys. Rev. Lett.* **71** 204
[22] Milman V Y, Stelmashenko N A and Blumenfeld R 1994 *Prog. Mater. Sci.* **38** 425
[23] McAnulty P, Meisel L V and Cote P J 1992 *Phys. Rev.* A **46** 3523
[24] Broek D 1974 *Elementary Engineering Fracture Mechanics* (Amsterdam: Noordhoff)
[25] Narayan O and Fisher D S 1992 *Phys. Rev. Lett.* **68** 3615
[26] Narayan O and Fisher D S 1992 *Phys. Rev.* B **46** 11 520
[27] Narayan O and Fisher D S 1993 *Phys. Rev.* B **48** 7030

[28] Nattermann T, Stepanow S, Tang L-H and Leshhorn H 1992 *J. Physique* II **2** 1483
[29] Halpin-Healy T and Zhang Yi-Cheng 1995 *Phys. Rep.* **254** 215 and references therein
[30] Ertaş D and Kardar M 1992 *Phys. Rev. Lett.* **69** 929
Ertaş D and Kardar M 1993 *Phys. Rev.* E **48** 1228
Ertaş D and Kardar M 1994 *Phys. Rev. Lett.* **73** 1703
[31] Ertaş D and Kardar M 1994 *Phys. Rev.* E **49** R2532
[32] Ertaş D and Kardar M 1996 *Phys. Rev.* B **53** 3520
[33] Bouchaud J-P, Bouchaud E, Lapasset G and Planès J 1993 *Phys. Rev. Lett.* **71** 2240
Bouchaud E, Bouchaud J-P, Planès J and Lapasset G 1993 *Fractals* **1** 1051
[34] Bouchaud E and Navéos S 1995 *J. Physique* I **5** 547
[35] Daguier P, Hénaux S, Bouchaud E and Creuzet F 1996 *Phys. Rev.* E **53** 5637
[36] Daguier P and Bouchaud E 1996 *Fracture-Instability Dynamics, Scaling, and Ductile/Brittle Behavior; MRS Fall Meeting (Boston, MA, 1995)* vol 409, ed R L Blumberg-Selinger, J J Mecholsky, A E Carlsson and E R Fuller (Pittsburgh, PA: MRS) p 343
[37] Nakano A, Kalia R K and Vashishta P 1994 *Phys. Rev. Lett.* **73** 2336
[38] Nakano A, Kalia R K and Vashishta P 1995 *Phys. Rev. Lett.* **75** 3138
[39] Nakano A, Kalia R K and Vashishta P 1996 *Fracture-Instability Dynamics, Scaling, and Ductile/Brittle Behavior; MRS Fall Meeting (Boston, MA, 1995)* vol 409, ed R L Blumberg-Selinger, J J Mecholsky, A E Carlsson and E R Fuller (Pittsburgh, PA: MRS) p 11
[40] Kalia R K, Nakano A, Omeltchenko A, Tsuruta K and Vashishta P 1997 *Preprint*
[41] Mandelbrot B B and Van Ness J W 1968 *SIAM Rev.* **10** 422
[42] Schmittbuhl J, Vilotte J P and Roux S 1995 *Phys. Rev.* E **51** 131
[43] Hansen A, Engoy T and Måly K J 1994 *Fractals* **2** 527
[44] Kardar M, Parisi G and Zhang Y-C 1986 *Phys. Rev. Lett.* **56** 889
[45] Leshhorn H, Nattermann T, Stepanow S and Tang L-H 1996 *Ann. Phys., Lpz.* at press
[46] Orignac E 1997 private communication
[47] Daguier P, Bouchaud E and Lapasset G 1995 *Europhys. Lett.* **31** 367
[48] Schmittbuhl J 1997 private communication
[49] Gao H and Rice J-R 1989 *J. Appl. Mech.* **56** 828
[50] Schmittbuhl J, Roux S, Vilotte J-P and Måly K J 1995 *Phys. Rev. Lett.* **74** 1787
[51] Thomas P B and Paczuski M 1996 *Phys. Rev. Lett.* submitted
[52] Sneppen K 1992 *Phys. Rev. Lett.* **69** 3539
[53] Maslov S and Paczuski M 1994 *Phys. Rev.* E **50** R643
[54] Roux S and Hansen A 1994 *J. Physique* I **4** 515
[55] Ramanathan S, Ertaş D and Fisher D S 1996 *Preprint* condmat 9611196
[56] Blackburn M J and Smith M P 1987 *US Patent* No 4716020
[57] Schmittbuhl J, Roux S and Berthaud Y 1994 *Europhys. Lett.* **28** 585
[58] Daguier P, Nghiem B, Bouchaud E and Creuzet F 1997 *Phys. Rev. Lett.* **78** 1062
[59] Sen S and Stebbins J F 1994 *Phys. Rev.* B **50** 822
[60] Gaskell P H, Eckersley M C, Barnes A C and Chieux P 1991 *Nature* **350** 675
[61] Ritchie R O and Bathe K J 1979 *Int. J. Fract.* **15** 47
[62] Lankford J and Davidson D L 1983 *Acta Metall.* **31** 1273
[63] Bathias C and Bailon J P 1980 *La Fatigue des Matériaux et des Structures* (Paris: Maloine)
[64] Hansen A, Hinrichsen E L and Roux S 1991 *Phys. Rev. Lett.* **66** 2476
[65] Roux S and François D 1991 *Scr. Metall.* **25** 1092
[66] Kardar M 1987 *Nucl. Phys.* B **290** 582
[67] Mézard M and Parisi G 1991 *J. Physique* I **1** 809
[68] Halpin-Healy T 1990 *Phys. Rev.* A **42** 711
[69] Batrouni G and Roux S 1997 *Preprint*
[70] Middleton A A 1995 *Phys. Rev.* E **52** R3337
[71] Nghiem B and Creuzet F 1997 private communication
[72] Fineberg J, Gross S P, Marder M and Swinney H L 1991 *Phys. Rev. Lett.* **67** 457
Fineberg J, Gross S P, Marder M and Swinney H L 1992 *Phys. Rev.* B **45** 5146
[73] Gross S P, Fineberg J, Marder M, McCormik W D and Swinney H L 1993 *Phys. Rev. Lett.* **71** 3162
[74] Boudet J F, Steinberg V and Ciliberto S 1995 *Europhys. Lett.* **30** 337
[75] Marder M and Gross S P 1995 *J. Mech. Phys. Solids* **43** 1
[76] Boudet J F, Ciliberto S and Steinberg V 1996 *J. Physique* II **6** 1493
[77] Ching E, Langer J S and Nakanishi H 1996 *Phys. Rev. Lett.* **76** 1087